







Taking the Monte-Carlo gamble: How not to buckle under the pressure!

Yessica K. Gomez¹  | Andrew M. Natale¹  | James Lincoff¹  |
Charles W. Wolgemuth²  | John M. Rosenberg³  | Michael Grabe¹ 

¹Cardiovascular Research Institute, Department of Pharmaceutical Chemistry, University of California, San Francisco, San Francisco, California, USA

²Departments of Molecular and Cellular Biology and Physics, University of Arizona, Tucson, Arizona, USA

³Department of Biological Sciences, University of Pittsburgh, Pittsburgh, Pennsylvania, USA

Correspondence

Michael Grabe, Cardiovascular Research Institute, Department of Pharmaceutical Chemistry, University of California, San Francisco, San Francisco, CA, USA.
Email: michael.grabe@ucsf.edu

John M. Rosenberg, Department of Biological Sciences, University of Pittsburgh, Pittsburgh, PA, USA.
Email: jmr@pitt.edu

Charles W. Wolgemuth, Departments of Molecular and Cellular Biology and Physics, University of Arizona, Tucson, AZ, USA.
Email: wolg@arizona.edu

Funding information

National Institutes of Health, Grant/Award Numbers: 4T32HL007731-25, R01-GM117593, R01-GM089740, R01-GM137109; National Science Foundation, Grant/Award Number: 2034836

Abstract

Consistent buckling distortions of a large membrane patch ($200 \times 200 \text{ \AA}$) are observed during molecular dynamics (MD) simulations using the Monte-Carlo (MC) barostat in combination with a hard Lennard–Jones (LJ) cutoff. The buckling behavior is independent of both the simulation engine and the force field but requires the MC barostat-hard LJ cutoff combination. Similar simulations of a smaller patch ($90 \times 90 \text{ \AA}$) do not show buckling, but do show a small, systematic reduction in the surface area accompanied by $\sim 1 \text{ \AA}$ thickening suggestive of compression. We show that a mismatch in the way potentials and forces are handled in the dynamical equations versus the MC barostat results in a compressive load on the membrane. Moreover, a straightforward application of elasticity theory reveals that a minimal compression of the linear dimensions of the membrane, inversely proportional to the edge length, is required for buckling, explaining this differential behavior. We recommend always using LJ force or potential-switching when the MC barostat is employed to avoid undesirable membrane deformations.

KEYWORDS

barostat, curvature, lipid bilayer, molecular dynamics, Monte-Carlo

We observed consistent undesirable distortions of a membrane patch during molecular dynamics (MD) simulations in Amber18 using the Monte-Carlo (MC) barostat¹ in combination with a standard 10 \AA hard Lennard–Jones (LJ) cutoff as recently mentioned by Im and colleagues²; here we report our successful efforts to ameliorate this problem by employing force-switching (FS). The MC barostat, which is currently implemented in Amber and OpenMM, is a relatively new barostat that is frequently used for constant pressure simulations as it reproduces the correct volume fluctuations, unlike the Berendsen

barostat,³ and it does not require the virial to be computed at every time step, unlike most barostats.¹ Meanwhile, a 9 or 10 \AA hard cutoff for nonbonded interactions is commonly employed to improve simulation speed, as explicitly recommended for use with Amber force fields. When these parameters are used to simulate a $200 \times 200 \times 80 \text{ \AA}$ box, we observe significant rapid buckling of an initially flat membrane into an egg carton pattern that then breaks xy-symmetry to relax into a sinusoidal plane wave, as shown in Figure 1.

After this initial observation, we ran a series of test simulations using different MD engines to isolate which parameter combinations correlate with membrane distortions (Supplementary Table A1), comparing the MC algorithm with (1) the widely available but

Yessica K. Gomez, Andrew M. Natale, and James Lincoff have done equal contribution to this article.

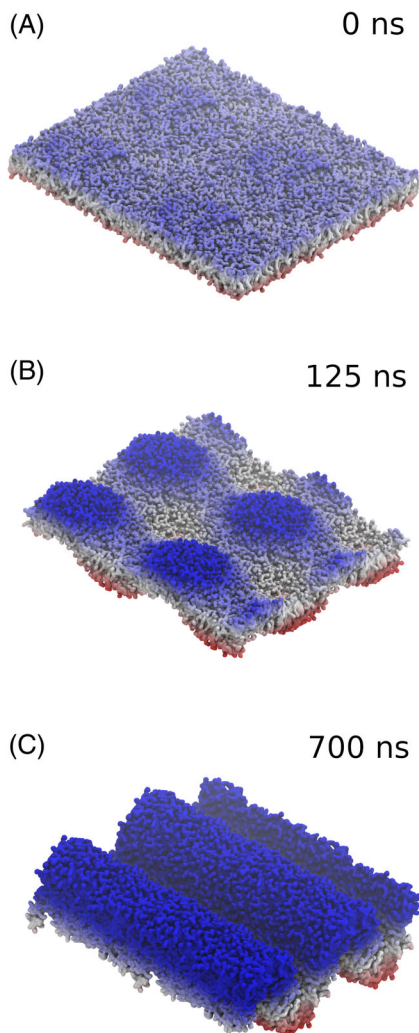


FIGURE 1 Membrane deformation induced by MC barostat and 10 Å cutoff. A 200 × 200 Å patch of POPC membrane with the hydrophobic lipid tails colored cyan and the head groups colored by height (z-coordinate—Blue positive, red negative). Note that all three panels show a 2 × 2 array of four simulation cells. (A) The initially flat membrane at the start of production exhibits minor height fluctuations. (B) By 125 ns, the membrane has buckled into an egg cartoon shape (see text). (C) By 700 ns, buckling has continued into nearly a steady state shape (see text)

problematic, Berendsen barostat and (2) the Parrinello-Rahman barostat⁴ implementation in Gromacs, which like the MC algorithm properly samples volume fluctuations. All simulations used semi-isotropic pressure scaling with coupling in the initial plane of the membrane (x–y plane) independent of the perpendicular axis. Examination of the box dimensions over time reveals that all simulations keep a constant volume (Supplementary Figure A1), albeit with up to 3% initial variation in the first few time steps in some cases; however, the MC barostat when used in combination with a 10 Å hard cutoff always results in a gradual compression of the x–y plane, and corresponding expansion along z, on the 100-ns time-scale (yellow traces in Figure 2A–C), leading to deformations like those shown in Figure 1.

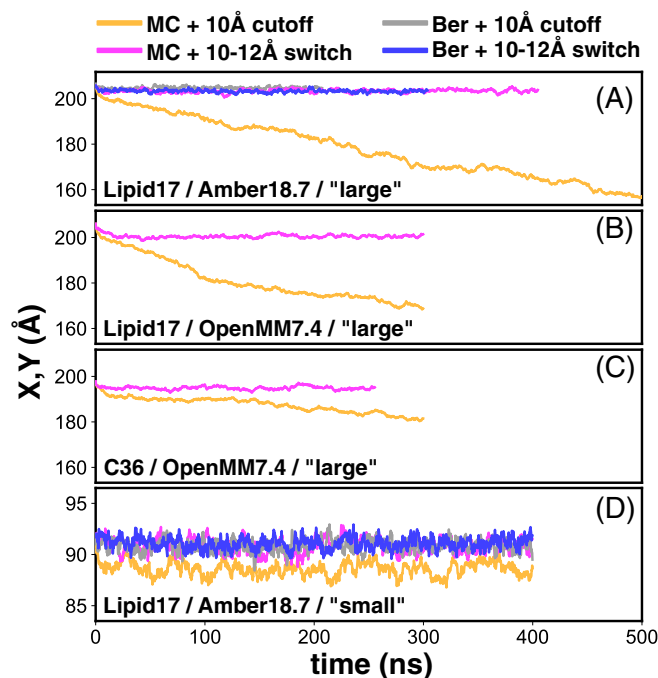


FIGURE 2 Changes in x/y-box dimensions over time for different combinations of system parameters. The identical length and width (x, y) of the membrane patches are plotted against time. The color key at the top defines combinations of barostats (MC-MC barostat or Ber-Berendsen) with LJ treatments (10 Å cutoff or 10–12 Å force switching). Each panel shows results for additional model combinations: (A) large membrane patch (initially 200 × 200 Å, Amber18.7 engine, and Lipid17 force field (#1–#4); (B) large patch, OpenMM7.4 engine, and Lipid17 (#9,#10); (C) large patch, OpenMM7.4 engine, and CHARMM36 force field (#11,#12); and (D) small patch (initially 90 × 90 Å, Amber18.7 engine, and Lipid17 (#15,#17,#18,#20). All numbers refer to simulations in Supplementary Information Table A1

Importantly, this phenomenon is not an artifact of a particular MD engine or force field as the buckling is reproduced in OpenMM as well as simulations performed with CHARMM36 (Supplementary Table A1), though CHARMM force fields are explicitly recommended for use with FS only. This suggests that the origin of the problem lies with the pairing of the MC barostat and a 10 Å (or shorter) LJ cutoff in membrane simulations. No other parameter combinations in Supplementary Table A1 resulted in significant membrane deformation.

We note that most published simulations employing the MC barostat in combination with a short LJ cutoff use smaller membrane patches, and they appear to be free of the distortions described above. We therefore tested whether 90 × 90 Å bilayers undergo buckling and found that they do not (Supplementary Table A1 and Supplementary Figure A1F). That said, the MC barostat simulation with 10 Å LJ cutoff does experience a 2 Å decrease of the x and y dimensions (yellow trace in Figure 2D) and a corresponding ~1 Å thickening of the width as if the membrane is under compression. Taken together, the extreme buckling observed on the large membrane patches coupled with the modest compression of the smaller patch suggests that there is an effective compressive force in the

membrane plane when the semi-isotropic MC barostat is used with a hard cutoff.

Changes to the LJ parameters are known to impact atomistic properties, including the particularly sensitive lipid density. Specifically, a hard LJ truncation of 10 Å reduces long range attraction compared to, say, a 10–12 Å switching distance, and might be expected to lead to a greater area-per-lipid (APL), as it does for the Berendsen barostat simulations (#3 and #4 in Supplementary Table A1). Why then does the MC barostat compress membranes when a short hard cutoff is employed? We believe that this arises from an inconsistency between the way forces and potentials are handled in the MC trial box-size change stage versus the dynamics stage. The MC barostat uses the potentials between pairs of atoms to determine whether a random box rescaling is energetically favorable. For a given configuration, atoms separated by a distance greater than the cutoff have zero interaction energy. However, in the dynamics steps, it is the force between atom pairs that is set to zero outside the cutoff distance, which is equivalent to a potential that is a negative constant for distances greater than the cutoff distance. These two corresponding LJ potential energy profiles are radically different (Supplemental Figure A2), with the MC barostat energy (potential U^2 in Supplemental Figure A2) containing an effective step change in the potential favoring smaller pairwise distances. This inconsistency between the assumed potentials in the MC and the MD steps leads to a discrepancy between the target equilibrium lipid densities in the bilayer, with a higher target density in the MC steps compared to the dynamics, introducing an effective compressive bias in the XY plane (see Supplementary Information Section 3).

We believe the problematic systems then evolve as follows. The flattened, effective potential employed during dynamics leads to lower in-plane lipid density by promoting out-of-plane lipid fluctuations resulting in membrane thickening. Meanwhile, the MC barostat favors higher in-plane lipid densities than the dynamics biasing volume trial moves toward compression of the xy-area over expansion. This area reduction exacerbates the crowding experienced during dynamics and the bilayer further thickens. This positive feedback cycle continues, eventually buckling the membrane. By using potential or force switching, even over very short distances, the target densities are consistent with one another, and the effective compression is removed so the membranes do not buckle (Supplementary Table A1, see simulation #9 vs. #25–27). Importantly, this process does not occur when a hard cutoff is employed with either the Berendsen or the Parrinello-Rahman barostats because they calculate the pressure from the virial, which uses MD forces—not energies—to drive changes in the box size based on the difference from the target pressure.

Next we employed an elastic energy model of the membrane that includes an energetic cost for in-plane compression together with a Helfrich-like bending energy⁵ to attempt to understand why small membranes only compress while large membranes buckle (see Supplementary Information Section 1 and Reference 6). According to this model, buckling occurs when the x/y cell dimensions decrease to the point where bending is more energetically favorable than in-plane

compression, giving a quantitative relationship for when that threshold is reached (Supplementary Information Equation (9)). When combined with the estimate of compressive strain induced by employing the MC barostat with a hard cutoff (Supplementary Information Equation (19)), we arrive at an expression that predicts the critical membrane length (L_{critical}) beyond which initially planar membrane patches of length (L_0) buckle:

$$L_0 > L_{\text{critical}} = \sqrt{\frac{\pi\kappa R^4}{4\rho_0^2\epsilon\lambda^6}} \propto R^2 \quad (1)$$

where κ is the bilayer bending modulus, ρ_0 is the initial lipid density (the inverse of the APL), ϵ and λ are the well depth and radius, respectively, of the LJ potential, and R is the applied LJ cutoff distance.

Putting this together, the compressive bias stresses the membrane, and that stress tends to grow with repetitive applications of the Metropolis algorithm until either the induced strain balances the effective compressive load or the membrane buckles. Compressive elastic balance is achieved quickly with the small ($L_0 = 90$ Å) membrane patch by a simple elastic compression. Equation (1) yields an L_{critical} value of 190 Å for a 10 Å hard LJ cutoff and the parameters of our simulations, correctly predicting that the small patch would not buckle while the 200 Å patch would. We conducted additional simulations to test these ideas (see Supplementary Information) including simulations with an 8 Å hard cutoff ($L_{\text{critical}} = 122$ Å) and a 12 Å hard cutoff ($L_{\text{critical}} = 274$ Å), and the results are all consistent with Equation (1). For example, a 200×200 Å patch with a 12 Å cutoff does not buckle, although it does show in-plane compression (#21 in Supplementary Table A1).

In conclusion, the extreme membrane distortions discussed here for the larger membrane patches only occur when using the MC barostat in combination with a 10 Å or less LJ cutoff; simply using a switching function avoids this undesirable result. While smaller patches do not undergo extreme distortion, they do deviate from experimentally derived parameters due to the effective compression; for instance, the APL shrinks from 68.7 ± 0.9 Å² to 65.7 ± 0.9 Å² when changing from a switching function to a hard cutoff (see #17 and #15 in Supplementary Information Table A1), with the former being in general agreement with the experimental value of 68.3 ± 1.5 Å^{2,7} but not the latter. These results raise a cautionary note regarding any membrane-containing simulation employing the MC barostat coupled with a hard LJ cutoff, and additional analysis would be needed to determine how other properties are impacted such as lipid-protein interactions or properties of mixed bilayers.

1 | METHODS

Initial atomic coordinates were generated using the CHARMM-GUI bilayer builder module.⁸ The “large” system contained 1200 POPC lipids, 53,866 water molecules with 0.15 M KCl, and had initial dimensions of $202 \times 202 \times 85$ Å³. The “small” system contained 240 POPC lipids, 10,766 water molecules with 0.15 M KCl and had initial dimensions of

$90 \times 90 \times 85 \text{ \AA}^3$. These structures were used to prepare all simulations. Two parameter sets were used in this study: (1) the Amber Lipid17⁹ force field with TIP3P water¹⁰ and Joung-Cheatham ions¹¹ (collectively referred to as “Lipid17” or “L17” throughout), or (2) the CHARMM36 lipid force field¹² with CHARMM TIP3P water¹⁰ and standard CHARMM ions (collectively referred to as “CHARMM36” or “C36” throughout).

From the starting coordinates, we initiated five separate equilibration runs: (a) “large” system with the Lipid17 forcefield in the Amber engine¹³; (b) “large” system with the CHARMM36 forcefield in the Amber engine; (c) “large” system with the CHARMM36 forcefield in the OpenMM engine¹⁴; (d) “large” system with the CHARMM36 forcefield in the Gromacs engine¹⁵; and (e) “small” system with the Lipid17 forcefield in the Amber engine. Heavy atoms were restrained with a force constant of $1.0 \text{ kcal/mol/\AA}^2$, and restraints were eased stepwise over 125 ps, followed by 20 ns of unrestrained dynamics. During equilibration, treatment of Van der Waals forces was done according to what is considered standard for the force field, that is, for CHARMM36 Lennard-Jones (LJ) forces were switched smoothly to zero in the range 10–12 Å, while for Lipid17 a plain cutoff of 10 Å was used. For equilibration of all simulations, a Berendsen barostat was used. All equilibration and production simulations used semi-isotropic pressure coupling requiring the x and y dimensions of the simulation cell to scale together while z scaled freely, a target pressure of 1 atm, a 2 fs timestep, and in all cases, long range electrostatic interactions were treated using the Particle Mesh Ewald method.¹⁶ Water molecules were kept rigid using the SETTLE algorithm,¹⁷ and bonds to hydrogen atoms were converted to rigid constraints using either the SHAKE¹⁸ (Amber and OpenMM) or LINCS¹⁹ (Gromacs) algorithms. All simulations in Amber and OpenMM used a Langevin thermostat with a friction coefficient of 1 ps^{-1} , while those in Gromacs used a Berendsen thermostat during equilibration and thereafter a Nose-Hoover thermostat. In all cases temperature was maintained at 310 K. Simulations using a MC barostat applied trial moves to the box vectors once per every 100 dynamics steps.

Each of the five equilibrated systems (coordinates, velocities, and box vectors) was used as the common starting point for several production trajectories with different settings and parameters outlined in Supplementary Table A1 and here in the main text.

ACKNOWLEDGMENTS

We would like to thank William DeGrado for first noticing the initial distortions and prompting us to explore the cause. This work was supported by a National Science Foundation Graduate Research Fellowship (YKG) and National Institutes of Health grants R01-GM089740, R01-GM117593, R01-GM137109, and Postdoctoral fellowship 4T32HL007731-25 (JL).

DATA AVAILABILITY STATEMENT

The data that support the findings of this study are available from the corresponding author(s) upon reasonable request.

ORCID

Yessica K. Gomez  <https://orcid.org/0000-0002-3976-5209>

Andrew M. Natale  <https://orcid.org/0000-0002-6320-0216>

James Lincoff  <https://orcid.org/0000-0003-3090-1240>

Charles W. Wolgemuth  <https://orcid.org/0000-0002-3588-3136>

John M. Rosenberg  <https://orcid.org/0000-0001-7616-4376>

Michael Grabe  <https://orcid.org/0000-0003-3509-5997>

REFERENCES

- [1] J. Åqvist, P. Wennerström, M. Nervall, S. Bjelic, B. O. Brandsdal, *Chem. Phys. Lett.* **2004**, 384(4–6), 288.
- [2] J. Lee, M. Hitznerberger, M. Rieger, N. R. Kern, M. Zacharias, W. Im, *J. Chem. Phys.* **2020**, 153(3), 035103.
- [3] H. J. Berendsen; J. Postma, W.F. van Gunsteren; A DiNola, J. R Haak. *J. Chem. Phys.* **1984**, 81(8), 3684–3690.
- [4] M. Parrinello, A. Rahman, *J. Appl. Phys.* **1981**, 52(12), 7182.
- [5] W. Helfrich, *Z. Naturforsch [C]* **1973**, 28(11), 693.
- [6] J. Eid, H. Razmazma, A. Jraj, A. Ebrahimi, L. Monticelli, *J. Phys. Chem. B* **2020**, 124(29), 6299.
- [7] N. Kučerka, S. Tristram-Nagle, J. F. Nagle, *J. Membrane Biol.* **2006**, 208(3), 193.
- [8] J. Lee, X. Cheng, J. M. Swails, M. S. Yeom, P. K. Eastman, J. A. Lemkul, S. Wei, J. Buckner, J. C. Jeong, Y. Qi, S. Jo, V. S. Pande, D. A. Case, C. L. Brooks, A. D. MacKerell, Jr., J. B. Klauda, W. Im, *J. Chem. Theory Comput.* **2016**, 12(1), 405–413.
- [9] C. J. Dickson, B. D. Madej, A. A. Skjerve, R. M. Betz, K. Teigen, I. R. Gould, R. C. Walker, *J. Chem. Theory Comput.* **2014**, 10(2), 865.
- [10] W. L. Jorgensen, J. Chandrasekhar, J. D. Madura, R. W. Impey, M. L. Klein, *J. Chem. Phys.* **1983**, 79(2), 926.
- [11] I. S. Joung, T. E. Cheatham, *J. Phys. Chem. B* **2008**, 112(30), 9020.
- [12] J. B. Klauda, R. M. Venable, J. A. Freites, J. W. O'Connor, D. J. Tobias, C. Mondragon-Ramirez, I. Vorobyov, A. D. MacKerell, R. W. Pastor, *J. Phys. Chem. B* **2010**, 114(23), 7830.
- [13] D. A. Case, (University of California, San Francisco, **2015**).
- [14] P. Eastman, J. Swails, J. D. Chodera, R. T. McGibbon, Y. Zhao, K. A. Beauchamp, L. P. Wang, A. C. Simmonett, M. P. Harrigan, C. D. Stern, R. P. Wiewiora, B. R. Brooks, V. S. Pande, *PLoS Comput. Biol.* **2017**, 13(7), e1005659.
- [15] M. J. Abraham, T. Murtola, R. Schulz, S. Páll, J. C. Smith, B. Hess, E. Lindahl, *SoftwareX* **2015**, 1, 19.
- [16] T. Darden, D. York, L. Pedersen, *J. Chem. Phys.* **1993**, 98(12), 10089.
- [17] S. Miyamoto, P. A. Kollman, *J. Comput. Chem.* **1992**, 13(8), 952.
- [18] J. P. Ryckaert, G. Ciccotti, H. J. C. Berendsen, *J. Comp. Phys.* **1977**, 23, 327.
- [19] B. Hess, H. Bekker, H. J. C. Berendsen, J. G. E. M. Fraaije, *J. Comput. Chem.* **1997**, 18(12), 1463.

SUPPORTING INFORMATION

Additional supporting information may be found in the online version of the article at the publisher's website.

How to cite this article: Y. K. Gomez, A. M. Natale, J. Lincoff, C. W. Wolgemuth, J. M. Rosenberg, M. Grabe, *J. Comput. Chem.* **2021**, 1. <https://doi.org/10.1002/jcc.26798>

Supplementary Information: Taking the Monte Carlo gamble: How not to buckle under the pressure!

Yessica K. Gomez, Andrew M. Natale, James Lincoff,
Charles W. Wolgemuth*, John M. Rosenberg† and Michael Grabe‡

1 Elastic model of compression-induced membrane buckling

We consider a scenario where the cutoff on the LJ potential produces an artificial compression of the membrane that can cause buckling. To examine whether this explanation is sufficient to explain the observed effect, we use the simplest energetic model for the membrane, with energetic costs for compression and bending of the mid-plane of the membrane. If the unstressed membrane has infinitesimal area given by $dxdy$ and the stressed membrane has infinitesimal area $\sqrt{g}dxdy$, then we can define the areal compression energy as

$$\mathcal{E}_A = \frac{\sigma}{2} \int (\sqrt{g} - 1)^2 dxdy . \quad (1)$$

Here σ is an areal compression modulus. We also assume that the bending energy of the membrane is given by the standard Helfrich energy

$$\mathcal{E}_b = \frac{\kappa}{2} \int K^2 dxdy , \quad (2)$$

where κ is the bending modulus and K is the mean curvature.

*wolg@arizona.edu

†jmr@pitt.edu

‡michael.grabe@ucsf.edu

For a membrane that is uniformly compressed along the x and y dimensions by a uniform amount $\gamma = \Delta L/L$, where L is the uncompressed length of a side and ΔL is the change in length, and is buckled out of the plane by a small amount $\delta(x, y)$, the metric factor is given by

$$\sqrt{g} \approx 1 - 2\gamma + \frac{1}{2} \left(\left(\frac{\partial \delta}{\partial x} \right)^2 + \left(\frac{\partial \delta}{\partial y} \right)^2 \right), \quad (3)$$

the mean curvature is

$$K \approx \frac{1}{2} \left(\frac{\partial^2 \delta}{\partial x^2} + \frac{\partial^2 \delta}{\partial y^2} \right), \quad (4)$$

and the total energy is

$$\mathcal{E} \approx \frac{\sigma}{8} \int \left(\left(\frac{\partial \delta}{\partial x} \right)^2 + \left(\frac{\partial \delta}{\partial y} \right)^2 - 4\gamma \right)^2 dx dy + \frac{\kappa}{8} \int \left(\frac{\partial^2 \delta}{\partial x^2} + \frac{\partial^2 \delta}{\partial y^2} \right)^2 dx dy, \quad (5)$$

which to 2nd order in δ is

$$\mathcal{E} \approx -\sigma\gamma \int \left(\left(\frac{\partial \delta}{\partial x} \right)^2 + \left(\frac{\partial \delta}{\partial y} \right)^2 \right) dx dy + \frac{\kappa}{8} \int \left(\frac{\partial^2 \delta}{\partial x^2} + \frac{\partial^2 \delta}{\partial y^2} \right)^2 dx dy. \quad (6)$$

For a periodic distortion of the membrane with wave vector \mathbf{q} , the energy of this mode is

$$\mathcal{E} = \frac{\kappa}{8} |\mathbf{q}|^4 - \sigma\gamma |\mathbf{q}|^2. \quad (7)$$

Therefore, wavevectors with $|\mathbf{q}|^2 < 8\sigma\gamma/\kappa$ should be unstable and buckle. Since the largest wavelength (which corresponds to the smallest magnitude of the wavevector) is $\lambda = L$, the instability should occur when

$$\frac{4\pi^2}{L^2} < \frac{8\sigma\Delta L}{\kappa L}, \quad (8)$$

or

$$\Delta L > \frac{\pi^2 \kappa}{2\sigma L}. \quad (9)$$

The bending modulus for a membrane is estimated to be on order of $\kappa \sim 20.7 \text{ kT} \approx 8.5 \times 10^{-10} \text{ N}\text{\AA}$ and the areal compression modulus is $\sigma \approx 2.13 \times 10^{-11} \text{ N}/\text{\AA}$ (Supplementary Table A2). Therefore, for a square patch of membrane with side of length $L = 90 \text{ \AA}$, we estimate that $\Delta L > 2.2 \text{ \AA}$ in order to induce buckling, whereas for $L = 200 \text{ \AA}$, we predict $\Delta L > 1 \text{ \AA}$ will cause the membrane to buckle.

2 Area-per-lipid (APL) calculations

The area-per-lipid (APL) headgroup is an important property of bilayers. Experimental values for POPC APL are: $68.3 \pm 1.5 \text{ \AA}^2$ [1], $64.3 \pm 1.3 \text{ \AA}^2$ (at 303 K), $67.3 \pm 1.3 \text{ \AA}^2$ (at 323 K) [2]. Computationally, the CHARMM36 POPC APL values presented here are comparable to the experimental values (see Supplementary Table A1) and consistent with published CHARMM-GUI benchmarks in the range of $64.0 - 66.1 \text{ \AA}^2$ (simulated at 303.15 K) [3, 4]. The Amber POPC APL value is $65.6 \pm 0.5 \text{ \AA}^2$ [5]. This published value is technically for Lipid14, as there is no published reference for Lipid17; however, we believe the Lipid17 POPC parameters are identical to Lipid14.

3 How potential cutoffs lead to compression in the MC barostat

We propose that a mismatch between the force and the potential that is used for the MC barostat is the cause of compression in lipid bilayer simulations (and consequently buckling of large bilayers). Consider forces arising from Lenard Jones potentials where a hard cutoff is used (e.g., particles at distances greater than 10 \AA do not interact). This corresponds to a potential energy that is constant, but not zero, at distances greater than the cutoff distance. This is different than a true potential cutoff, where the pair-wise potential energy abruptly goes to zero at the cutoff distance. If the MC barostat ignores the potential between particles at distances larger than the cutoff distance, then the potential energy that leads to the dynamic forces in the system will be inconsistent with the potential that is assumed by the MC barostat.

To determine how this affects the membrane, we note that since the force is the gradient of the potential energy, if the force abruptly goes to zero, then the potential goes to a constant. We, therefore, consider the two potential energies, U^1 and U^2 , shown below. Both potentials are a Lennard Jones potential for distances less than the cutoff distance R . At distances greater than the cutoff distance, U^1 is equal to the potential at R , $U^1(r > R) = U^1(R) = -c$, while $U^2(r > R) = 0$.

For simplicity, we will assume a 2D membrane comprised of N molecules that is contained within a box with sides L . If we can treat each molecule as being similar, then the total potential energy of the system is just N times the

integral over the membrane area of the pairwise potential times the density distribution of the molecules surrounding a specific molecule. That is, the total potential energy is

$$U_T = \pi N^2 \int p(r) U(r) r dr , \quad (10)$$

where $p(r)$ is the probability distribution for two particles to be separated by the distance r . For particles that are sufficiently far away, we expect that $p(r) \approx 1/L^2$. The total potential energy for the two potentials shown above is then

$$\begin{aligned} U_T^1 &\approx U_0 - \frac{\pi N^2 c}{L^2} (L^2 - R^2) = U_0 - \pi N c (N - \rho R^2) , \\ U_T^2 &= U_0 , \end{aligned} \quad (11)$$

where $\rho = N/L^2$,

$$U_0 = \pi \epsilon N^2 \int_0^R p(r) \left[\left(\frac{\lambda}{r} \right)^{12} - \left(\frac{\lambda}{r} \right)^6 \right] r dr , \quad (12)$$

for an LJ potential of strength ϵ and minimum energy at $r_{\min} = 2^{1/6} \lambda$. The approximately equal to sign in the first equation represents that the probability densities $p(r)$ are only approximately equal for U^1 and U^2 . We define the equilibrium density for this potential to be ρ_0 . For small deviations away from this density, the potential can be approximated as being quadratic in the areal strain, $(A - A_0)/A_0 = (\rho_0 - \rho)/\rho$, and consequently, approximately quadratic in the density:

$$U_0 \approx \frac{\sigma L_0^2}{2} \left(\frac{\rho_0}{\rho} - 1 \right)^2 \approx \frac{\sigma L_0^6}{2 N^2} (\rho_0 - \rho)^2 , \quad (13)$$

where σ is the areal compressibility modulus, $L_0 = \sqrt{N/\rho_0}$ is the equilibrium box size for this potential, and ρ is the current density.

From these definitions, the equilibrium densities for the two potentials can be found from

$$\begin{aligned} \frac{\partial U^1}{\partial \rho} &= \frac{\partial U_0}{\partial \rho} + \pi N c R^2 = \frac{\sigma L_0^6}{N^2} (\rho - \rho_0) + \pi N c R^2 , \\ \frac{\partial U^2}{\partial \rho} &= \frac{\partial U_0}{\partial \rho} = \frac{\sigma L_0^6}{N^2} (\rho - \rho_0) . \end{aligned} \quad (14)$$

Therefore, the potential U^1 , which is the potential energy consistent with the dynamic forces in the simulations, has a different equilibrium density than the hard cutoff potential assumed by the MC barostat, such that the equilibrium density for the dynamics is

$$\rho'_0 = \rho_0 - \frac{\pi N^3 c R^2}{\sigma L_0^6} . \quad (15)$$

If we define the equilibrium box size for U1 to be L , we can rewrite this as

$$\frac{N}{L^2} = \frac{N}{L_0^2} - \frac{\pi N^3 c R^2}{\sigma L_0^6} , \quad (16)$$

or

$$\frac{L_0^2}{L^2} = \left(1 - \frac{\pi N^2 c R^2}{\sigma L_0^4} \right) , \quad (17)$$

and the compressive strain imposed by the MC barostat is

$$\frac{L_0}{L} - 1 \approx -\frac{\pi N^2 c R^2}{2\sigma L_0^4} . \quad (18)$$

Using that $c = -U^1(R) \approx 4\epsilon (\lambda/R)^6$,

$$\frac{L_0}{L} - 1 \approx -\frac{2\pi N^2 \epsilon \lambda^6}{\sigma L_0^4 R^4} . \quad (19)$$

We can estimate a magnitude of the imposed strain using the following parameters: $N = 1200$ (number of lipids simulated on the 200 Å box size), $R = 10$ Å, $\sigma = 2 \times 10^{-11}$ N/Å, and $L_0 = 200$ Å, along with approximate parameters for the CHARMM carbon atoms C27 and C36, $\lambda = 4$ Å and $\epsilon = 0.02$ kcal/mol = 5×10^{-11} N Å(per atom). With these parameters, we find

$$\frac{L_0}{L} - 1 \approx \frac{7}{640} = -0.011 . \quad (20)$$

Therefore, the MC barostat with a hard cutoff on the potential imposes an approximately 1% compressive strain on the system, which is consistent with what we see in the 90 Å × 90 Å simulation and is sufficient to buckle the membrane in the 200 Å × 200 Å simulation.

These results can be combined to obtain an estimate of the critical box size at which we expect the MC barostat to induce buckling under given hard

cutoff simulation conditions as follows: Equation 9 above gives the amount of compression required to cause the membrane to buckle and equation 19 gives an estimate of the amount of compressive strain induced by the MC barostat. Therefore setting equation 9 equal to L times equation 19 and solving for the critical box size, $L_{critical}$, gives the result shown below, which is identical to equation 1 in the main text:

$$L_{critical} = \sqrt{\frac{\pi\kappa R^4}{4\rho_0^2\epsilon\lambda^6}} \quad (21)$$

Here κ , R , ϵ and λ are as above. $\rho_0 = \frac{N}{L_0^2}$ where N is the number of lipids and L_0 is the initial box size. That is, ρ_0 is the initial areal lipid number density i.e. the reciprocal of the initial area per lipid (APL). Note that $L_{critical} \propto R^2$. This result predicts that the membrane will buckle whenever the initial box size, $L_0 > L_{critical}$.

Supplementary Table A1. Description of all molecular simulations.

Simulation # (equilibration) ^(a)	System size	Force-field	Engine	Barostat	LJ cutoff treatment ^(b)	Used isotropic LJ dispersion correction ^(c)	Production length (ns)	Trajectory average properties over final 50 ns (\pm standard deviation)					Membrane buckles?
								Box X,Y (Å)	XY APL (Å ²) ^(d)	Box Z (Å)	Density (g/mL)	Potential energy (kcal/mol $\times 10^5$)	
1 (A)	322,686 atoms ("Large" - 1200 POPC lipids)	Lipid17	Amber 18.17	Monte Carlo	10 Å hard cutoff	yes	670	158.9 (± 0.9)	42.1 (± 0.5)	123.8 (± 1.4)	1.0061 (± 0.0008)	-7.763 (± 0.005)	yes
2 (A)		Lipid17	Amber 18.17	Monte Carlo	10-12 Å force-switching	no	405	203.5 (± 0.8)	69.0 (± 0.5)	75.9 (± 0.6)	1.0007 (± 0.0009)	-7.714 (± 0.005)	no
3 (A)		Lipid17	Amber 18.17	Berendsen	10 Å hard cutoff	yes	207	204.7 (± 0.5)	69.9 (± 0.4)	75.3 (± 0.4)	0.9966 (± 0.0006)	-7.745 (± 0.005)	no
4 (A)		Lipid17	Amber 18.17	Berendsen	10-12 Å force-switching	no	304	203.2 (± 0.5)	68.8 (± 0.3)	76.1 (± 0.4)	1.0004 (± 0.0006)	-7.713 (± 0.005)	no
5 (B)		CHARMM36	Amber 18.17	Monte Carlo	10 Å hard cutoff	yes	315	188.2 (± 0.7)	59.0 (± 0.5)	87.2 (± 0.7)	1.0180 (± 0.0009)	-5.504 (± 0.005)	yes
6 (B)		CHARMM36	Amber 18.17	Monte Carlo	10-12 Å force-switching	no	349	197.9 (± 0.6)	65.3 (± 0.4)	79.7 (± 0.5)	1.0078 (± 0.0009)	-5.407 (± 0.005)	no
7 (B)		CHARMM36	Amber 18.17	Berendsen	10 Å hard cutoff	yes	305	197.9 (± 0.6)	65.3 (± 0.4)	79.2 (± 0.5)	1.0131 (± 0.0006)	-5.493 (± 0.005)	no
8 (B)		CHARMM36	Amber 18.17	Berendsen	10-12 Å force-switching	no	200	197.8 (± 0.4)	65.2 (± 0.3)	79.7 (± 0.4)	1.0076 (± 0.0006)	-5.407 (± 0.005)	no
9 (A)		Lipid17	OpenMM 7.4	Monte Carlo	10 Å hard cutoff	yes	300	171.0 (± 1.5)	48.7 (± 0.8)	106.0 (± 1.8)	1.0146 (± 0.0009)	-7.847 (± 0.005)	yes
10 (A)		Lipid17	OpenMM 7.4	Monte Carlo	10-12 Å potential-switching	yes	300	200.5 (± 0.5)	67.0 (± 0.3)	77.0 (± 0.4)	1.0148 (± 0.0009)	-7.849 (± 0.005)	no
11 (B)		CHARMM36	OpenMM 7.4	Monte Carlo	10 Å hard cutoff	yes	300	182.5 (± 1.4)	55.5 (± 0.9)	92.4 (± 1.4)	1.0219 (± 0.0009)	-5.545 (± 0.005)	yes
12 (B)		CHARMM36	OpenMM 7.4	Monte Carlo	10-12 Å potential-switching	yes	255	194.6 (± 0.5)	63.1 (± 0.3)	81.2 (± 0.4)	1.0216 (± 0.0009)	-5.544 (± 0.005)	no
13 (C)		CHARMM36	Gromacs 2018.8	Parinello-Rahman	10 Å hard cutoff	no	73	196.1 (± 0.6)	64.1 (± 0.4)	80.7 (± 0.5)	1.0134 (± 0.0010)	-5.544 (± 0.007)	no
14 (C)		CHARMM36	Gromacs 2018.8	Parinello-Rahman	10-12 Å force-switching	no	200	196.9 (± 0.6)	64.6 (± 0.4)	80.2 (± 0.5)	1.0107 (± 0.0012)	-5.474 (± 0.007)	no
15 (D)	64,512 atoms ("Small" - 240 POPC lipids)	Lipid17	Amber 18.17	Monte Carlo	10 Å hard cutoff	yes	400	88.8 (± 0.6)	65.7 (± 0.9)	78.5 (± 1.1)	1.0147 (± 0.0020)	-1.566 (± 0.002)	no
16 (D)		Lipid17	Amber 18.17	Monte Carlo	10 Å hard cutoff	no	400	88.7 (± 0.5)	65.6 (± 0.7)	79.4 (± 0.9)	1.0054 (± 0.0019)	-1.548 (± 0.002)	no
17 (D)		Lipid17	Amber 18.17	Monte Carlo	10-12 Å force-switching	no	400	90.8 (± 0.6)	68.7 (± 0.9)	76.2 (± 0.9)	1.0006 (± 0.0022)	-1.539 (± 0.002)	no
18 (D)		Lipid17	Amber 18.17	Berendsen	10 Å hard cutoff	yes	400	90.9 (± 0.5)	68.8 (± 0.8)	75.1 (± 0.9)	1.0139 (± 0.0015)	-1.566 (± 0.002)	no
19 (D)		Lipid17	Amber 18.17	Berendsen	10 Å hard cutoff	no	400	91.9 (± 0.5)	70.4 (± 0.8)	74.8 (± 0.9)	0.9951 (± 0.0013)	-1.544 (± 0.002)	no
20 (D)		Lipid17	Amber 18.17	Berendsen	10-12 Å force-switching	no	400	91.3 (± 0.6)	69.4 (± 0.9)	75.4 (± 0.9)	1.0000 (± 0.0014)	-1.539 (± 0.002)	no
21 (A)	322,686 atoms ("Large" - 1200 POPC lipids)	Lipid17	Amber 18.17	Monte Carlo	12 Å hard cutoff	yes	303	199.9 (± 0.5)	66.4 (± 0.3)	78.2 (± 0.4)	1.0098 (± 0.0009)	-7.802 (± 0.005)	no
22 (A)		Lipid17	Amber 18.17	Monte Carlo	8 Å hard cutoff	yes	143	175.7 (± 2.8)	51.5 (± 1.6)	102.3 (± 3.3)	0.9966 (± 0.0009)	-7.682 (± 0.005)	yes
23 (A)		Lipid17	Amber 18.17	Monte Carlo	8-10 Å force-switching	no	227	206.9 (± 0.7)	71.3 (± 0.5)	74.4 (± 0.5)	0.9873 (± 0.0010)	-7.603 (± 0.005)	no
24(A)		Lipid17	Amber 18.17	Monte Carlo	9.5-10 Å force-switching	no	192	204.9 (± 1.0)	70.0 (± 0.7)	75.3 (± 0.7)	0.9936 (± 0.0009)	-7.655 (± 0.005)	no
25 (A)		Lipid17	OpenMM 7.4	Monte Carlo	8-10 Å potential-switching	yes	300	202.3 (± 0.6)	68.2 (± 0.4)	75.8 (± 0.5)	1.0142 (± 0.0009)	-7.846 (± 0.005)	no
26 (A)		Lipid17	OpenMM 7.4	Monte Carlo	9.5-10 Å potential-switching	yes	300	201.0 (± 0.6)	67.3 (± 0.4)	76.7 (± 0.4)	1.0148 (± 0.0009)	-7.849 (± 0.005)	no
27 (A)		Lipid17	OpenMM 7.4	Monte Carlo	9.95-10 Å potential-switching	yes	300	200.3 (± 0.7)	66.9 (± 0.5)	77.2 (± 0.5)	1.0148 (± 0.0009)	-7.849 (± 0.005)	no

(a) - All production trajectories marked by the same letter shared a common equilibration phase and thus began with the same initial coordinates, velocities, and box vectors.

(b) - Typical LJ cutoff treatment options differ by engine and force field; CHARMM force field documentation recommends using a force-switching scheme; OpenMM lacks the option to apply force-switching but includes options for a potential-switching scheme.

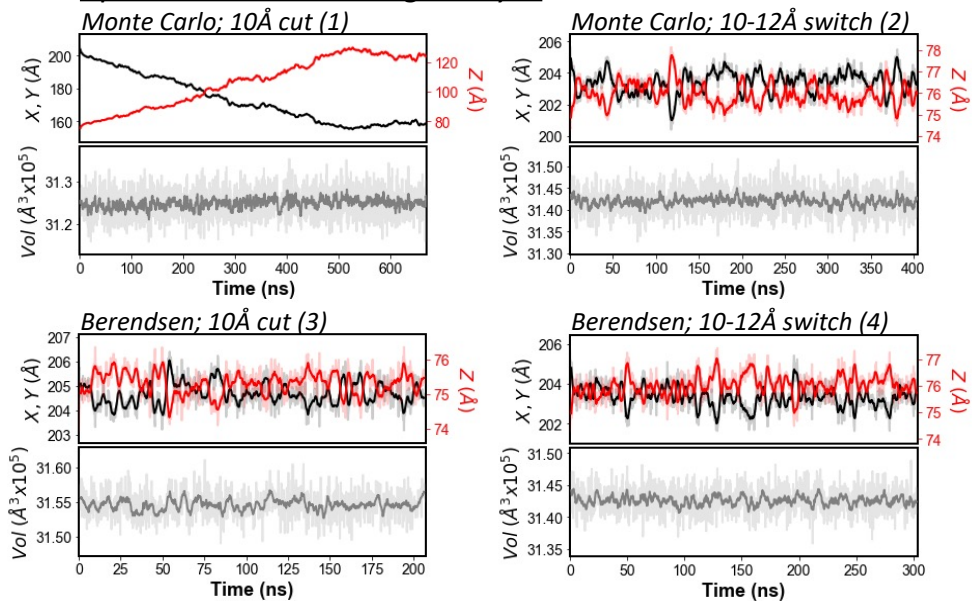
(c) - The use of an isotropic dispersion correction to approximately account for interactions beyond the cutoff differs by engine and force field; CHARMM force field documentation recommends not applying such a correction for simulations of lipid bilayers; The Amber engine uses such a correction by default - however it is automatically turned off when the force-switching scheme is active.

(d) - Here area per lipid (APL) is simply calculated as the area of the simulation box in X and Y divided by the number of lipids per leaflet.

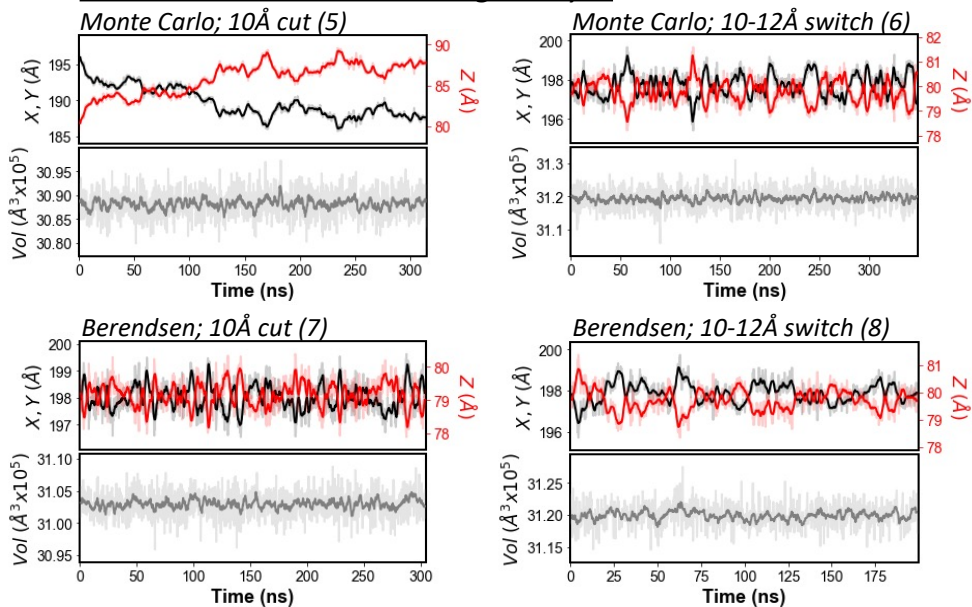
Supplementary Table A2: Membrane biophysical properties.

Parameter	Value	Reference
Bending modulus	$8.5 \times 10^{-10} N\text{\AA}$	[6]
Areal compression modulus	$2.13 \times 10^{-11} N/\text{\AA}$	[6]

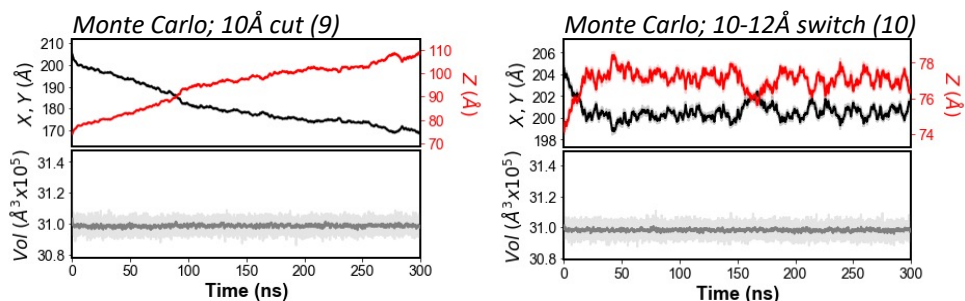
A Lipid17 in Amber18; large bilayer



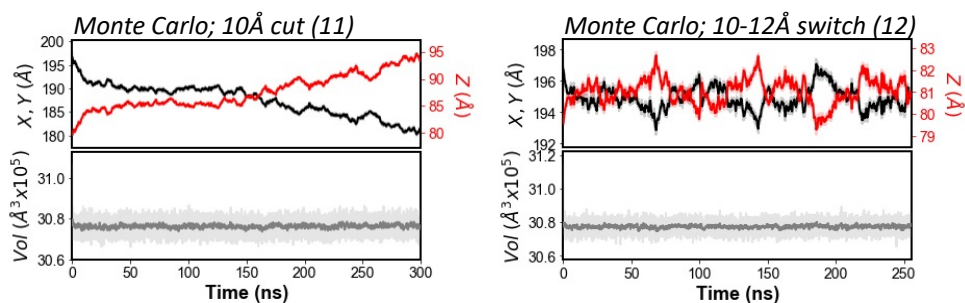
B CHARMM36 in Amber18; large bilayer



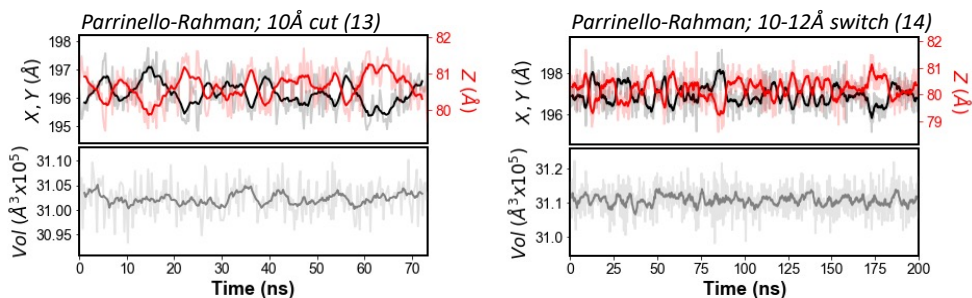
C Lipid17 in OpenMM 7.4; large bilayer



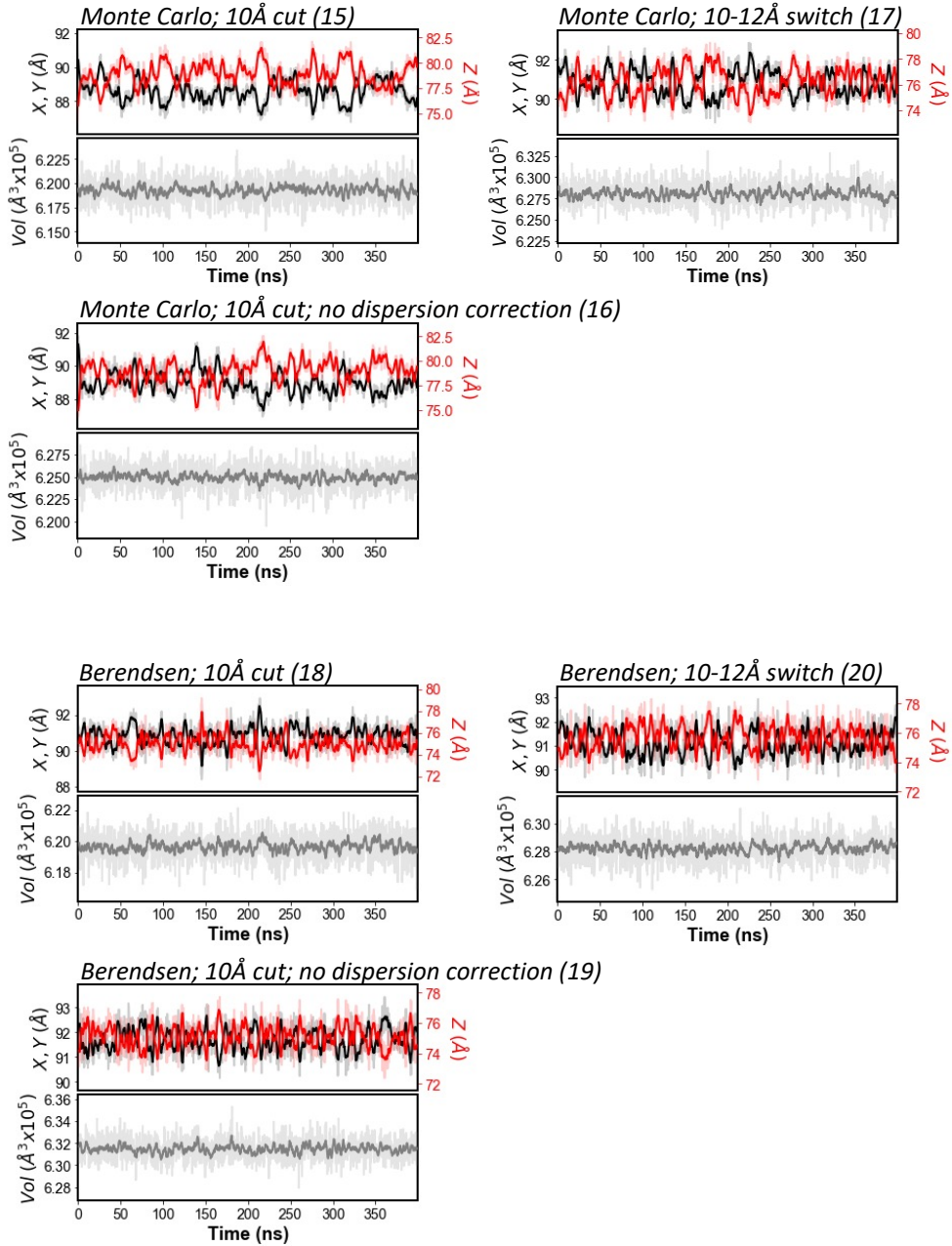
D CHARMM36 in OpenMM 7.4; large bilayer



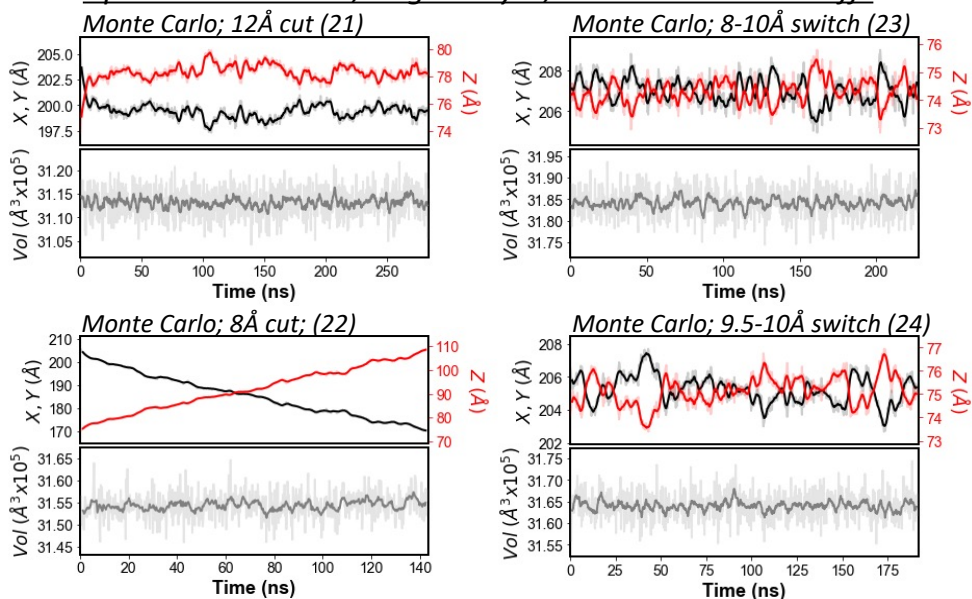
E CHARMM36 in GROMACS 2018.8; large bilayer



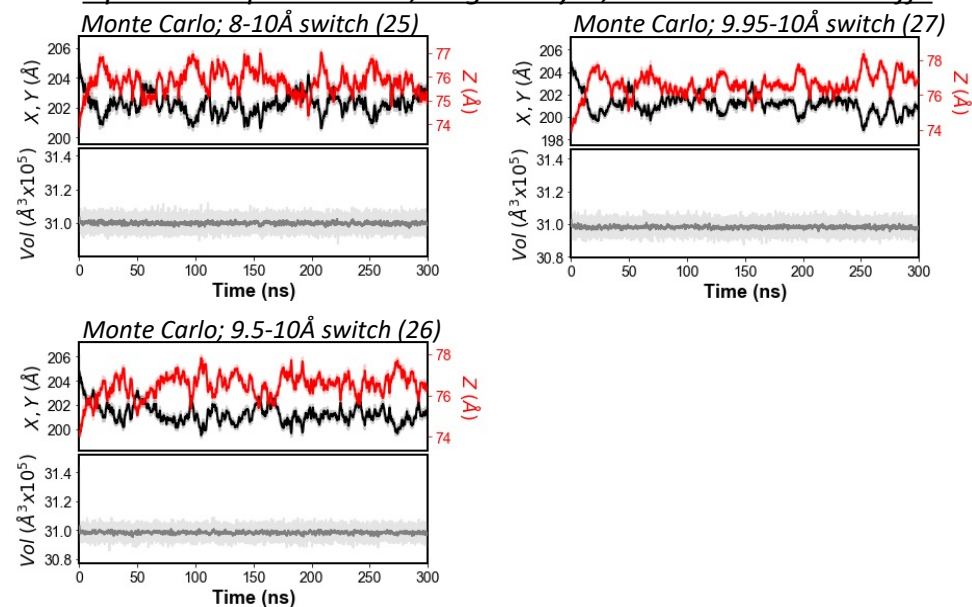
F Lipid17 in Amber18; small bilayer



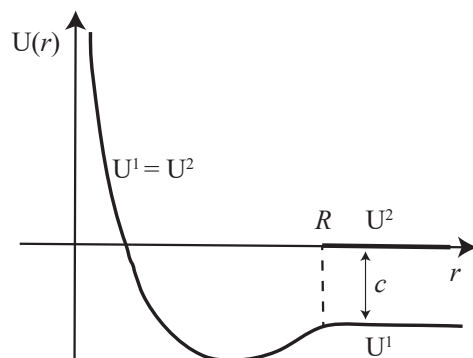
G Lipid17 in Amber18; large bilayer; MC + alternate cutoffs



H Lipid17 in OpenMM 7.4; large bilayer; MC + alternate cutoffs



Supplementary Figure A1: Changes in xy dimension, z value, and box volume over time for different combinations of system parameters. Membrane/box lengths and widths (x,y)_{1,2} are identical. Colors corresponds to values on the left or right ordinate. Each panel (A-G) corresponds to the indicated combination lipid force field, molecular dynamics engine, and the initial size of the membrane patch. The specific combination of barostat and LJ treatment are indicated at the top of each plot along with the identifying simulation number used in Supplementary Table A1.



Supplementary Figure A2: Two representative potentials U^1 and U^2 . Both potentials are a Lennard Jones potential for $r \leq R$. For $r > R$, the first potential is constant with $U^1(r > R) = U^1(R)$, representing the potential for a hard cutoff on the force, while $U^2(r > R) = 0$, which represents a hard cutoff on the potential.

References

- [1] N. Kucerka, S. Tristram-Nagle, J.F. Nagle, *J Membrane Biol* **2006**, *208*, 193.
- [2] N. Kucerka, M.P. Nieh, J. Katsaras, *BBA - Biomem* **2011**, *1808*, 2761.
- [3] J. Lee et al., *J Chem Theory Comp* **2016**, *12*, 405.
- [4] J.B. Klauda et al., *J Phys Chem B* **2010**, *114*, 7830.
- [5] C.J. Dickson, B.D. Madej, A.A. Skjevik, R.B. Betz, K. Teigen, I.R. Gould, R.C. Walker, *J Chem Theory Comp* **2014**, *10*, 865.
- [6] D. Argudo, N.P. Bethel, F.V. Marcoline, C.W. Wolgemuth, M. Grabe *Biophys J* **2017**, *112*, 2159.